Conference on Modelling Fluid Flow (CMFF'22)
The 18th International Conference on Fluid Flow Technologies
Budapest, Hungary, August 30-September 2, 2022

Direct Numerical Simulation of the Wake Flow of a Miniature Vortex Generator and its Interaction with a Laminar Boundary Layer

Maarten VANIERSCHOT[1], András SZABÓ[2], Péter Tamás NAGY[2], György PAÁL[2]

[1] Corresponding Author. KU Leuven, Department of Mechanical Engineering, Group T Leuven campus, Celestijnenlaan 300, B-3001 Heverlee, Belgium. Tel.: +32 16 301072, E-mail: maarten.vanierschot@kuleuven.be
[2] Department of Hydrodynamic Systems, Faculty of Mechanical Engineering, Budapest University of Technology and Economics. E-mail: aszabo@hds.bme.hu

ABSTRACT

Miniature vortex generators (MVGs) are an attractive technology to delay laminar to turbulent transition or to postpone flow separation of laminar boundary layers. Despite the appearance of several recent studies, much more work still needs to be done to optimize these MVGS or to study their interaction with a boundary layer flow. Therefore, in this study we perform Direct Numerical Simulations (DNS) to study the complex three dimensional wakes generated by a pair of triangular and rectangular winglets and their interaction with a laminar boundary layer flow. Vortex identification using the Q-criterion shows the existence of a strong pair of counter-rotating vortices. Next to this primary vortex pair, much weaker secondary vortices can also be found, induced by the winglet geometry. For five Blasius profiles with different boundary layer thicknesses, the strength, radius and position of the main vortex pair is characterized. The generated output profiles of this study can be used as an input for solving the boundary region equations further downstream and together with a BiGlobal stability analysis, the effectiveness of the MVGs in the suppression of Tollmien-Schlichting waves can be examined.

Keywords: Boundary layer interaction, DNS, Miniature Vortex Generators, Wake flow

NOMENCLATURE

p	$[Pa]$	pressure
R	$[m]$	radius
r	$[m]$	distance from the vortex center
R^2	$[-]$	coefficient of determination
r_f	$[-]$	refinement ratio
U, V, W	$[m/s]$	streamwise, wall normal, spanwise velocity component
u_i	$[m/s]$	velocity component in the i-direction
U_∞	$[m/s]$	freestream velocity
V_m	$[m/s]$	velocity magnitude
x, y, z	$[m]$	streamwise, wall normal, spanwise coordinate
δ	$[m]$	boundary layer thickness
Γ	$[m^2/s]$	circulation
ν	$[m^2/s]$	kinematic viscosity
ρ	$[kg/m^3]$	density

Subscripts and Superscripts

c	vortex center
θ	polar coordinate

1. INTRODUCTION

The application of streamwise streaks to a boundary layer flow can increase the transitional Reynolds number as these streaks can dampen the formation of Tollmien-Schlichting waves, since it is well-known that these waves can undergo secondary instabilities, leading to a transition to turbulence of the boundary layer [1]. Hence, suppressing them can shift the transition location downstream and therefore reduce the skin friction drag. Nevertheless, if the streak amplitude is too large, an inflectional instability of the boundary layer occurs, bypassing the classical transition mechanism [2]. Therefore, special care must be taken in the generation of streamwise streaks. From a practical point of view, the streaks can be generated by applying structural disturbances in the boundary layer, such as for instance cylinders or bumps. However, care must be taken as their wakes might also exhibit unsteady behavior, reducing the effectiveness [3]. A promising technology to generate high amplitude streaks are winglets, the so-called Miniature Vortex Generators (MVGs) [4],[5],[6]. They are implemented in pairs to gen-

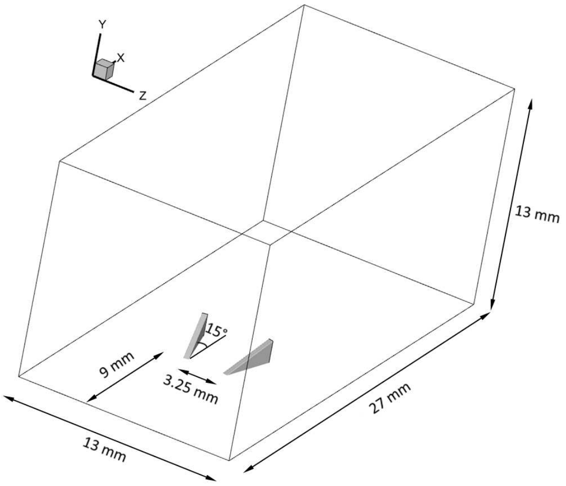

Figure 1. Schematic view of the numerical domain for the triangular MVGs

erate a counter rotating vortex pair. MVGs can be triangular or rectangular in shape and they have been studied extensively. Nevertheless, a detailed comparison of the flow field generated by rectangular or triangular MVGs is still lacking, as is also the influence of the boundary layer thickness on the flow structures in their wakes. To fill this knowledge gap, this study compares the flow fields generated by triangular and rectangular MVGs and studies their wake structure as a function of the boundary layer thickness. The generated output profiles of this study can be used as an input for BiGlobal stability analyses, where the effectiveness of the MVGs in the suppression of Tollmien-Schlichting waves can be examined [7].

2. NUMERICAL SETUP

2.1. MVG geometry

The MVG configuration in this study is based on the work of Siconolfi et al. [8]. A schematic view of the triangular MVG configuration is shown in Figure 1. The numerical domain is a rectangular box with length $X = 27$ mm, height $Y = 13$mm and width $Z = 13$mm, where the x-axis is the flow direction and the origin of the cartesian coordinate system is located at the inlet of the domain on the bottom wall, halfway the spanwise direction. The MVGs are placed in the center of a cross-sectional plane at a distance of 9mm from the inlet. The MVGs have a length of 3.25 mm, a width of 0.3 mm and a height of 1.3 mm. The distance between the MVG pair is 3.25 mm and they are placed under an angle of 15° with the flow direction. These MVGs are placed in pairs along the spanwise direction with a distance of 13 mm between them.

2.2. Governing equations

In this study, the steady state 3D Navier-Stokes equations for Newtonian fluids are solved. The equations, representing the conservation of mass and momentum are given by

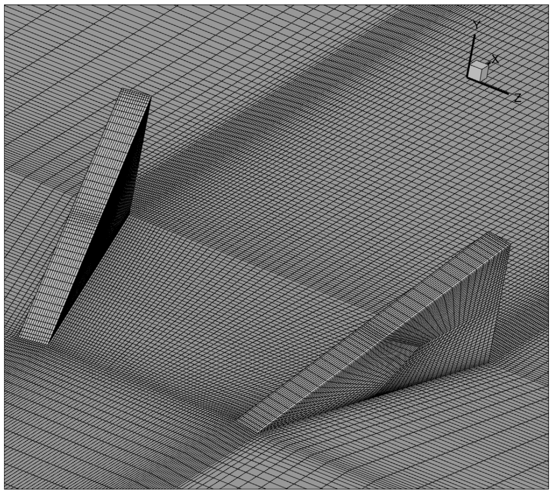

(a) Triangular MVG pair

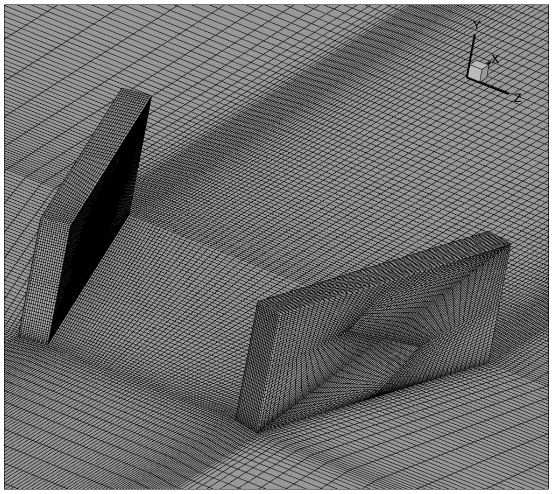

(b) Rectangular MVG pair

Figure 2. Details of the surface mesh of the MVG pair.

$$\frac{\partial u_j}{\partial x_j} = 0 \text{ and} \tag{1}$$

$$u_j \frac{\partial u_i}{\partial x_j} = -\frac{1}{\rho}\frac{\partial p}{\partial x_i} + \nu \frac{\partial^2 u_i}{\partial x_j \partial x_j}, \tag{2}$$

where u_i is a velocity component, ν is the kinematic viscosity, ρ is the density and p is the pressure. In this study, the governing fluid is air at standard temperature and pressure with a density $\rho = 1.225\, kg/m^3$ and a kinematic viscosity of $\nu = 1.4607\, mm^2/s$. The equations are solved using Ansys Fluent 18.2. The numerical grid is hexahedrally structured and constructed using PointWise. The total number of cells is around 2 million. A view of the surface mesh of the rectangular and triangular MVGs is shown in Figure 2. To maintain a similar grid structure between the two types, the rectangular winglet is divided in two triangles.

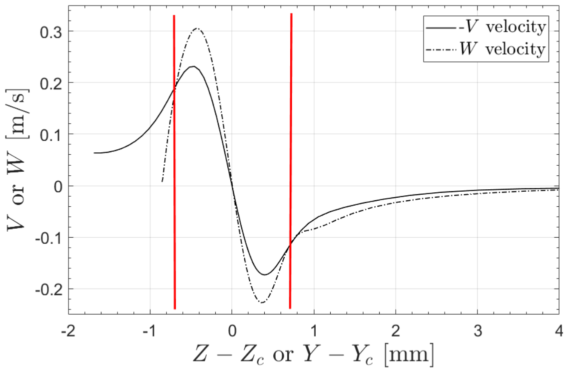

Figure 3. Horizontal and vertical velocity profiles through the center of the vortex in a cross-sectional plane x =22 mm

2.3. Boundary conditions

At the inlet, a fully developed Blasius velocity profile in the wall normal coordinate (y) is adopted and uniform in the spanwise direction (z). The freestream velocity is $U_\infty = 7.7$ m/s and the boundary layer thicknesses simulated are $\delta = 0$, 0.65, 1.3, 2.6 and 3.25 mm, giving a Reynolds number based on the thickness between 0 and 1713. At the outlet, a pressure boundary condition is applied where the gauge pressure is set at 0 Pa. On the side walls, periodic boundary conditions are applied and the top boundary is a symmetry plane.

2.4. Solution strategy

The QUICK (Quadratic upstream interpolation for convective kinematics) discretization scheme for momentum is adopted, while the pressure is discretised by the PRESTO! scheme [9, 10]. The segregated SIMPLEC (Semi-Implicit Method for Pressure Linked Equations-Consistent) is used for pressure velocity coupling. For each simulation, the residuals levels drop down to double precision machine accuracy before the iterations are stopped.

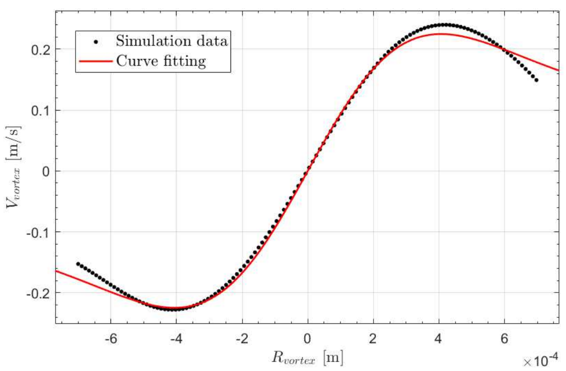

Figure 4. Average of the horizontal and vertical velocity profiles through the center of the vortex in a cross-sectional plane x =22 mm

2.5. Vortex characterisation

In order to determine the characteristics of each vortex pair generated by the MVGs, a Batchelor vortex is fitted to the velocity profiles along a horizontal and vertical line through the vortex center in a plane at $x = 22$ mm. An example of such numerically obtained profiles is shown in Figure 3. Although the difference between the local velocity maximum location of V and W is very small, it can be clearly seen that the vortex is slightly asymmetric due to effects of the bottom wall and the other vortex of the pair. Therefore, the fitted Batchelor vortex is applied to the average of both profiles between ±0.7 mm from the center (red lines in the figure). An example of such an averaged profile is shown in Figure 4.
The velocity profile of a Batchelor vortex is given by

$$V_\theta(r,\theta) = \frac{\Gamma}{2\pi r}\left[1 - \exp\left(-r^2/R_c^2\right)\right], \quad (3)$$

where V_θ is the V component for a horizontal profile or the W component for a vertical profile, r is the distance from the vortex center, Γ the circulation and R_c the radius of the vortex. The fitted Batchelor vortex based on the 2 profiles given in Figure 3 is shown by the red curve in Figure 4. The R^2 value is 0.9971 for this particular profile and the lowest value found in this study was 0.98, showing a Batchelor vortex profile is a very good fit for both the rectangular and triangular MVGs.

3. RESULTS

3.1. Mesh independency study

To estimate the discretisation error, the Grid Convergence index (GCI) method developed by Roache is employed [11]. The relative error between different meshes is calculated as

$$\epsilon = \frac{\phi_1 - \phi_2}{\phi_1}, \quad (4)$$

where ϕ is a certain flow quantity and the subscript 1 refers to the coarser mesh and 2 refers to the finer mesh. The GCI on the coarse mesh can be calculated as

$$GCI = 3\epsilon\frac{r_f^p}{r_f^p - 1}, \quad (5)$$

where r_f is the refinement ratio in one direction ($r_f = \sqrt{2}$ in this study) and p is the order of the discretisation scheme, which is 3 in this case. Three different grids, a coarse, medium and fine mesh were

Table 1. Number of cells for the three meshes employed in the grid convergence study

coarse mesh	medium mesh	fine mesh
2,009,421	5,715,812	16,075,368

Table 2. Location, strength and radius of the vortex pair of the triangular MVG for the three meshes employed in a cross-sectional plane x =22 mm

	coarse mesh	medium mesh	fine mesh
Y_c [mm]	0.8539	0.8529	0.8528
Z_c [mm]	1.6436	1.6424	1.6434
Γ [mm^2/s]	802	787	814
R_o [mm]	0.3624	0.3539	0.3637

adopted for which Table 1 shows the number of grid cells of each. The values of the location, strength and radius of the right vortex of the pair is shown in Table 2. The results show a non-monotonic convergence and the GCI of Y_c for the coarse mesh is 0.4% and for the medium mesh it is 0.04%, while for Z_c the GCI is 0.2% for both the coarse and medium meshes. The difference between the values for the circulation and radius is larger, but they fall well within the 95% confidence interval of the fitting parameters of Eq. 3, which is about 4% .

3.2. Flow field structure

The flow field structure of the MVGs is shown in Figure 5 for a boundary layer thickness $\delta = 0$ at the inlet. The black surfaces denote zero streamwise velocity, hence recirculation zones, and vortical structures are visualised using the Q criterion [12]. Both MVGs generate a counter rotating vortex pair which is not aligned with the flow direction. However, the vortex pair generated by the rectangular pair spreads more compared to the triangular one. The structure of the flow field of the rectangular MVGs is also more complex compared to the triangular ones. In the former, apart from the primary counter rotation vortex pair, a secondary vortex pair is also present. Moreover, a horse shoe vortex is formed near the leading edge of the rectangular MVG, which is a typical structure observed in bluff body flows [13]. Looking at the wake structure, the wake of the rectangular MVG is also much more complicated. At the leading edge, a small recirculation zone can be observed, which is not present in the triangular MVG, as the triangular surface of the latter allows the air to flow smoothly around the MVG. The angle of attack of 15° induces separation on the inner side of the MVG pair. For the rectangular MVG, this wake is much larger (comparing Figure 6a with Figure 6b) and as a result, the drag coefficient of the triangular MVG, $C_D = 1.32$, is much smaller than the one for the rectangular MVG, $C_D = 2.58$. This large discrepancy is caused by a domination of the pressure drag due to separation over the viscous drag as the former is 4 times higher compared to the latter.

The flow field structure of both MVGs for a boundary layer thickness $\delta = 3.25$ mm ($\delta/h = 2.5$) is shown in Figure 7. Comparison with Figure 5 shows the large influence of the boundary layer thickness on

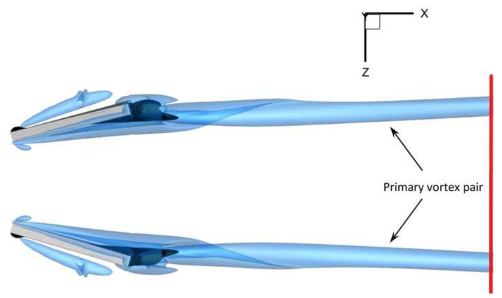

(a) Triangular MVGs

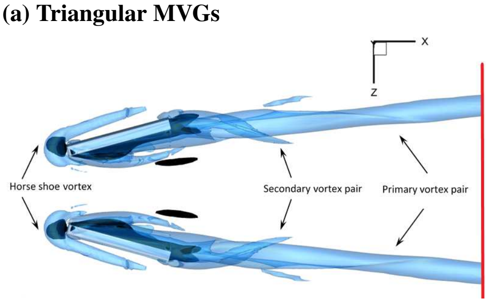

(b) Rectangular MVGs

Figure 5. Top view of the structure of the flow field of the MVGs for a boundary layer with thickness $\delta = 0$ mm. The black isosurface denotes zero streamwise velocity, while the vortical structures are visualised with blue isosurfaces of $Q = 8 \times 10^6$ 1/s

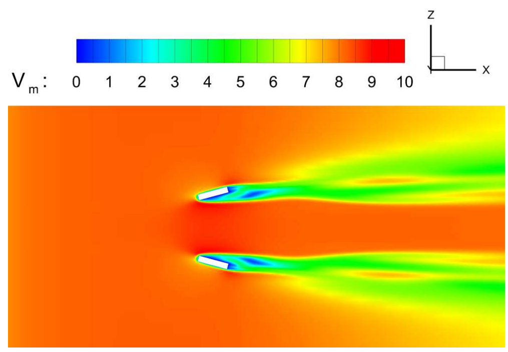

(a) Triangular MVGs

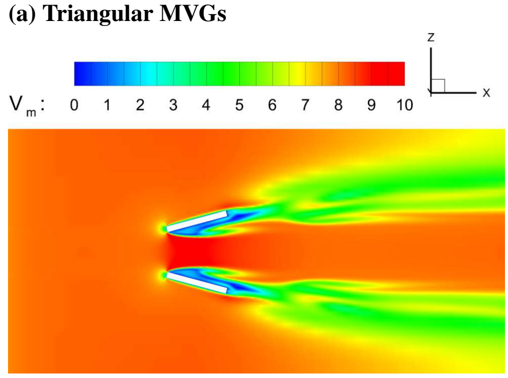

(b) Rectangular MVGs

Figure 6. Velocity magnitude in a cross-sectional plane at half the height of the MVG for a boundary layer with thickness $\delta = 0$ mm.

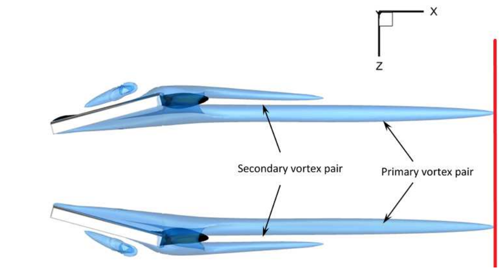

(a) Triangular MVGs

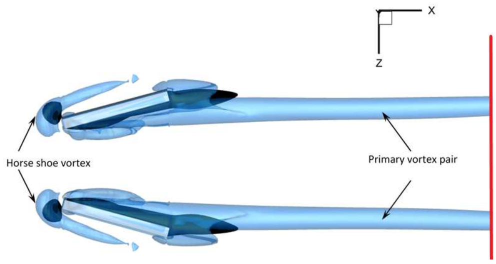

(b) Rectangular MVGs

Figure 7. Top view of the structure of the flow field of the MVGs for a boundary layer with thickness δ = 3.25 mm (δ/h = 2.5). The black isosurface denotes zero streamwise velocity, while the vortical structures are visualised with blue isosurfaces of Q = 8×10^5 1/s

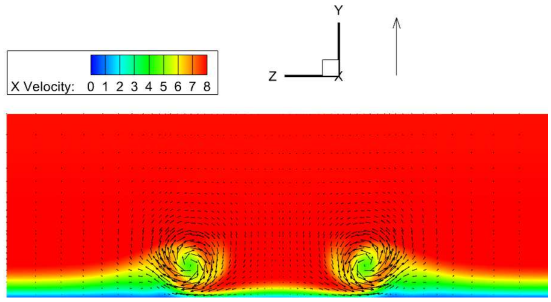

(a) Triangular MVGs

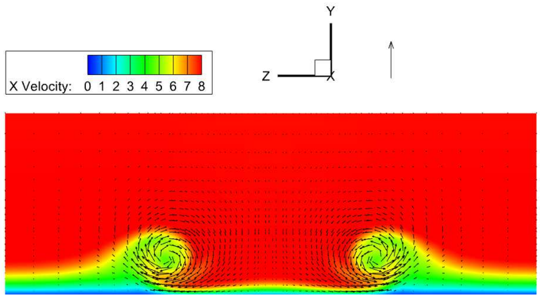

(b) Rectangular MVGs

Figure 9. Details of the vortex pair at a cross-sectional plane at x = 22 mm for a boundary layer of thickness δ = 0 mm. The length of the reference vector is 5 m/s

the flow field. Comparing Figures 5a and 7a shows

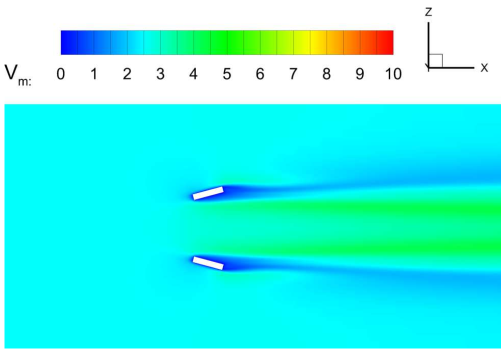

(a) Triangular MVGs

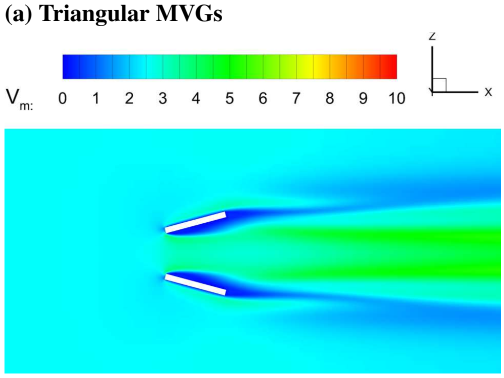

(b) Rectangular MVGs

Figure 8. Velocity magnitude in a cross-sectional plane at half the height of the MVG for a boundary layer with thickness δ = 3.25 mm.

a secondary vortex pair for the triangular MVG for δ = 3.25 mm (δ/h = 2.5). For the rectangular MVG, the complexity of the flow field is reduced and the secondary vortex pair is no longer present. Nevertheless, the horse shoe vortex at the leading edge is still present. Similar to $\delta = 0$ mm, the drag coefficient of the triangular MVG, C_D = 0.24, is much smaller than the one for the rectangular MVG, C_D = 0.56. This large discrepancy is again caused by a domination of the pressure drag due to separation (Figure 8) over the viscous drag, although it is only 2 times higher instead of 4 for δ = 0 mm. Nevertheless, as the wake is smaller (comparison of Figure 8 with Figure 6), the drag coefficient is significantly lower than for $\delta = 0$ mm.

3.3. Far field of the MVGs

The far field structure behind the MVGs, at a cross-sectional plane x = 22 mm (depicted by the red lines in Figures 5 and 7) for a boundary layer thickness δ = 0 mm is shown in Figure 9. The MVGs significantly reduce the boundary layer thickness in the region between the vortex pair, both for the rectangular and triangular MVGs. This reduction in thickness is much less if the boundary layer thickness at the inlet is increased, as shown in Figure 10.

3.4. Influence of the boundary layer thickness

As seen from Figures 5 and 7, the boundary layer thickness has a significant influence on the structure of the flow field and hence the characteristics of the

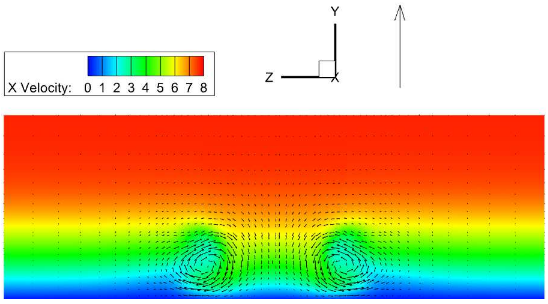

(a) Triangular MVGs

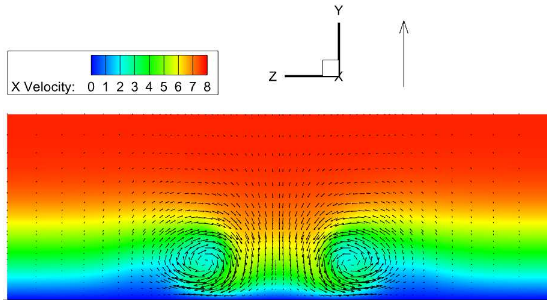

(b) Rectangular MVGs

Figure 10. Details of the vortex pair at a cross-sectional plane at x = 22 mm for a boundary layer of thickness δ = 3.25 mm. The length of the reference vector is 2 m/s

vortex pair. The location, strength and radius of the triangular MVG pair is shown in Table 3 and of the rectangular pair in Table 4. The values are obtained from a curve fit of Eq. 3 to the average velocity profiles of the horizontal and vertical direction through the vortex center. As the boundary layer thickness increases, the strength of the vortex pair decreases, as also the distance between the pair. This is related to the decrease in pressure difference between the front and rear side of the MVG as the incoming velocity profile along the height of the MVG decreases since the boundary layer thickness at the location of the MVG pair increases. A decrease in pressure difference generates a vortex pair, similar to the wing-tip vortices in airplane wings, which is less strong. Moreover, the rectangular MVGs generate a stronger vortex pair compared to the triangular MVGs.

4. CONCLUSIONS

In this study, direct numerical simulations of the fluid flow around rectangular and triangular Miniature Vortex Generators (MVGs) in a flat plate boundary layer flow are performed. The wake structure is analysed as a function of the boundary layer thickness δ. It is shown that the rectangular MVGs generate a more complex flow field for small δ, while the triangular MVGs have a more complex flow field for large δ. The vortex pair generated by the rectangular MVGs is also stronger than the triangular one. As δ increases, the vortex pair becomes less strong and the distance between the cores decreases. With the results in this study, the generated output profiles at x = 22 mm can be used as an input for solving the boundary region equations further downstream and together with a BiGlobal stability analysis, the effectiveness of the MVGs in the suppression of Tollmien-Schlichting waves can be examined.

Table 3. Vortex center, strength and radius of the vortex pair of the triangular MVG in a cross-sectional plane x =22 mm

δ	0	$0.5h$	h	$2h$	$2.5h$
Y_c $[mm]$	0.863	0.856	0.834	0.847	0.854
Z_c $[mm]$	2.11	1.97	1.83	1.68	1.64
Γ $[mm^2/s]$	3971	3038	2172	1106	802
R_c $[mm]$	0.322	0.299	0.314	0.336	0.362

Table 4. Vortex center, strength and radius of the vortex pair of the rectangular MVG in a cross-sectional plane x = 22 mm

δ	0	$0.5h$	h	$2h$	$2.5h$
Y_c $[mm]$	0.941	0.928	0.911	0.891	0.907
Z_c $[mm]$	2.55	2.38	2.18	1.85	1.76
Γ $[mm^2/s]$	5923	5364	4470	2366	1789
R_c $[mm]$	0.346	0.357	0.392	0.455	0.486

ACKNOWLEDGEMENTS

The authors wish to thank KU Leuven and Budapest University of Technology and Economics for financing this research through grant No. CELSA/21/024.

REFERENCES

[1] Herbert, T., 1988, "Secondary Instability of Boundary-layers", *Annu Rev Fluid Mech*, Vol. 20, pp. 487–526.

[2] Brandt, L., and Henningson, D., 2002, "Transition of Streamwise Streaks in Zero-pressure-gradient Boundary Layers", *J Fluid Mech*, Vol. 472, pp. 229–262.

[3] Loiseau, J.-C., Robinet, J.-C., and Cherubini, S. end Leriche, E., 2014, "Investigation of the Roughness-induced Transition: Global Stability Analyses and Direct Numerical Simulations", *J Fluid Mech*, Vol. 760, pp. 175–211.

[4] Fransson, J., and Talamelli, A., 2012, "On the Generation of Steady Streamwise Streaks in Flat-plate Boundary Layers", *J Fluid Mech*, Vol. 698, pp. 211–234.

[5] Shahinfar, S., Sattarzadeh, S., Fransson, J., and Talamelli, A., 2012, "Revival of Classical Vortex Generators now for Transition Delay", *Phys Rev Lett*, Vol. 109, p. 074501.

[6] Shahinfar, S., Fransson, J., Sattarzadeh, S., and Talamelli, A., 2013, "Scaling of Streamwise

Boundary Layer Streaks and their Ability to Reduce Skin-friction Drag", *J Fluid Mech*, Vol. 733, pp. 1–32.

[7] Szabó, A., Nagy, P., Vanierschot, M., and Paál, G., 2022, "Stability Analysis of a Streaky Boundary Layer generated by Miniature Vortex Generators", *to appear in: Proceedings of the 18th International Conference on Fluid Flow Technologies (CMFF22)*, Budapest, Hungary.

[8] Siconolfi, L., Camarri, S., and Fransson, J., 2015, "Stability Analysis of Boundary Layers Controlled by Miniature Vortex Generators", *J Fluid Mech*, Vol. 784, pp. 596–618.

[9] Leonard, B., 1979, "A Stable and Accurate Convective Modelling Procedure based on Quadratic Upstream Interpolation", *Comput Methods Appl Mech Eng*, Vol. 19, pp. 59–98.

[10] Patankar, S., 1980, *Numerical Heat Transfer and Fluid Flow*, Hemisphere, Washington DC.

[11] Roache, P., 1994, "Perspective: a Method for Uniform Reporting of Grid Refinement Studies", *J Fluids Eng*, Vol. 116, pp. 405–413.

[12] Jeong, J., and Hussain, F., 1995, "On the Identification of a Vortex", *J Fluid Mech*, Vol. 285, pp. 69–94.

[13] Carr, I., and Plesniak, M., 2017, "Surface obstacles in pulsatile flow", *Experiments in Fluids*, Vol. 58, p. 152.